Frictional Behavior of Atomically Thin Sheets: Hexagonal-Shaped Graphene Islands Grown on Copper by Chemical Vapor Deposition

Philip Egberts,[†,§] Gang Hee Han,[‡,⊥] Xin Z. Liu,[†] A. T. Charlie Johnson,[‡,*] and Robert W. Carpick[†,*]

[†]Department of Mechanical Engineering and Applied Mechanics, University of Pennsylvania, 220 South 33rd Street, Philadelphia, Pennsylvania 19104, United States and [‡]Department of Physics and Astronomy, University of Pennsylvania, 209 South 33rd Street, Philadelphia, Pennsylvania 19104, United States. [§]Present address: Department of Mechanical and Manufacturing Engineering, University of Calgary, 40 Research Place NW, Calgary Alberta, T2L 1Y6, Canada. [⊥]Present address: 85583, Center for Integrated Nanostructure Physics (CINAP), Sungkyunkwan University (SKKU), Suwon, South Korea.

ABSTRACT Single asperity friction experiments using atomic force microscopy (AFM) have been conducted on chemical vapor deposited (CVD) graphene grown on polycrystalline copper foils. Graphene substantially lowers the friction force experienced by the sliding asperity of a silicon AFM tip compared to the surrounding oxidized copper surface by a factor ranging from 1.5 to 7 over loads from the adhesive minimum up to 80 nN. No damage to the graphene was observed over this range, showing that friction force microscopy serves as a facile, high contrast probe for identifying the presence of graphene on Cu. Consistent with studies of epitaxially grown, thermally grown, and mechanically exfoliated graphene films, the friction force measured between the tip and these CVD-prepared films depends on the number of layers of graphene present on the surface and reduces friction in comparison to the substrate. Friction results on graphene indicate that the layer-dependent friction properties result from puckering of the graphene sheet around the sliding tip. Substantial hysteresis in the normal force dependence of friction is observed with repeated scanning without breaking contact with a graphene-covered region. Because of the hysteresis, friction measured on graphene changes with time and maximum applied force, unless the tip slides over the edge of the graphene island or contact with the surface is broken. These results also indicate that relatively weak binding forces exist between the copper foil and these CVD-grown graphene sheets.

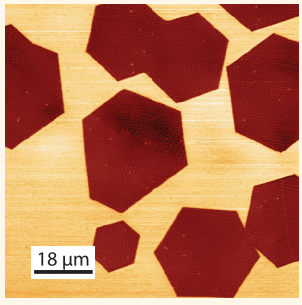

KEYWORDS: atomic force microscope (AFM) · graphene · copper · nanotribology · chemical vapor deposition (CVD)

Graphene, an atomically thin sheet of sp^2-bonded carbon, has the potential to revolutionize both the electronics industry and the longevity of micro- and nanomechanical devices. So far, high quality graphene can only be grown in large quantities by chemical vapor deposition (CVD) synthesis, a requirement for most engineering applications.[1,2] However, only recently has the chemical synthesis of graphene been achieved with sufficient quality, *e.g.*, free of defects or at least with defects that minimally affect its strength,[3] to be a viable alternative to other routes to graphene, including mechanical exfoliation[4] and thermal decomposition.[5] One primary motivating interest in graphene, beyond its impressive electrical properties, is the extraordinary mechanical properties, in particular the extremely high strength and stiffness,[3,6] as well as low friction.[7−9]

The frictional properties of graphene produced through both mechanical exfoliation[8] and thermal decomposition[7] show layer-dependent and substrate-dependent characteristics. In mechanically exfoliated graphene, the low out-of-plane bending elastic modulus compared to the in-plane elastic modulus has been proposed to result in the formation of an out-of-plane deformation around, and possibly in front of, the nanoscale sliding tip; this is referred to as the puckering mechanism and was observed for other few-layer 2D exfoliated sheets.[8] An increased resistance to out-of-plane deformation, and correspondingly, lower friction, was observed as the number of graphene layers was increased (reaching

* Address correspondence to cjohnson@physics.upenn.edu, carpick@seas.upenn.edu.

Received for review February 24, 2014 and accepted April 23, 2014.

Published online April 23, 2014
10.1021/nn501085g

the friction force value for bulk graphite at a thickness of approximately 4 layers), or when the strong adhesion between graphene and a high surface energy substrate (muscovite mica[10]) was present. Both effects reduce the ability of the graphene sheet to pucker. Under these conditions, friction was ~50% lower than compared to a monolayer on a low-adhesion substrate, or if freely suspended.[8] Molecular dynamics (MD) simulations of single asperities sliding on graphene sheets found that, given a sufficiently large graphene sheet, local deformation of the graphene sheet around the nanoscale asperity results in the same layer-dependent friction behavior.[11] In graphene sheets produced through thermal decomposition, two layers of graphene were found to have 50% lower friction compared to a single layer:[7] the mechanism was proposed to result from a layer-dependent electron–phonon coupling between the graphene and the substrate. Recently, it was shown that oxidized graphite/graphene can adhere to the tip, leading to a local delamination of the topmost graphene layer from the remaining surface.[12] In contrast to the aforementioned studies on pristine graphene, this local layer delamination increases friction compared to clean bulk graphite for adhesive loads only, *i.e.*, when unloading after first making contact. While different than the puckering mechanism, this increasing friction with decreasing load (negative differential friction coefficient) is also intimately related to the extremely low bending stiffness of graphene sheets.[12,13] It has also been reported that chemically modifying graphene with fluorine to form fluorinated graphene increases friction substantially; it was suggested that the higher bending stiffness of fluorinated graphene leads to this increased friction, in contrast to the effect lower bending stiffness has in the aforementioned studies.[14] All of these results indicate that while even a monolayer of graphene can substantially reduce the friction force a tip experiences when sliding against a surface, the origins of the friction reduction and the dependence on graphene thickness, substrate adhesion, growth method, and surface chemistry can be significant and require further study. Furthermore, there are relatively few studies examining the frictional properties of CVD graphene at present.[15,16]

The primary focus of this paper is to examine the friction-reducing characteristics of CVD graphene grown on polycrystalline copper substrates. This processing route has the advantage of being low cost compared to other synthesis routes.[1] Furthermore, recent atomic resolution scanning tunneling microscopy (STM) studies prove that high quality graphene sheets can be grown on copper single crystals[17−19] and polycrystalline copper,[3,20−23] and are of high quality and defect-free over large (micrometer) areas. Examination of graphene produced through this synthesis route can provide an informed understanding of the interplay between graphene and its supporting substrates.

Here, we examine frictional behavior of single and the first reported measurements on bilayer CVD graphene islands on copper compared against the surrounding exposed copper (oxide) surface. Examination of the load dependence of friction, both single and bilayer, shows that the friction properties of CVD grown graphene share common features to that observed in mechanically exfoliated graphene sheets, specifically, that friction is lower on bilayers than monolayers.[8] Furthermore, we also show that atmospheric pressure deposition of graphene on copper shows similar friction-reducing characteristics compared to the substrate as low-pressure graphene deposition on copper.[15] Finally, we show that the friction reducing characteristics of graphene on copper depend strongly on the sliding history, particularly when measuring friction without scanning over the edge of a graphene island, or pulling the tip out of contact with the graphene. These results further illustrate the frictional consequences of the high bending flexibility of graphene, which can result in nonreversible friction behavior.

RESULTS AND DISCUSSION

Frictional Behavior of Copper *vs* Graphene. Figure 1(A) shows a topographic image of the surface of a typical region of a CVD-grown sample on Cu deposited at a temperature of 1057 ± 1 °C. Previous studies on graphene produced through this method proved using Raman spectroscopy[24,25] that single layers of graphene are in fact covering the surface. Identification of the regions of the copper foil covered by graphene in this image is difficult, as the topography is dominated by the underlying large-scale roughness of the foil, which is typically 4.1 nm RMS as measured over a 20 × 20 nm^2 area. Figure 1(B) shows a line profile through the white dashed line shown in Figure 1(A). Despite taking this topographic line profile across both exposed and graphene-covered regions, no clear height change at the graphene edges is observed, although faint contrast lines at edges can be seen. In comparison, identification of graphene islands from the copper substrate is readily apparent in the friction force image, *i.e.*, the image generated by subtracting the lateral force images obtained in the forward and reverse directions, and subsequently scaling the difference by a factor of 0.5, in Figure 1(C). The dark regions correspond to areas of the foil covered by graphene islands that exhibit low friction, compared to the exposed parts of the foil. Using the friction image in Figure 1(C) to identify the graphene islands in Figure 1(A), those areas of sample covered by graphene often appear depressed in the topographic images. The depression of the graphene sheet compared to the surrounding copper surface results from

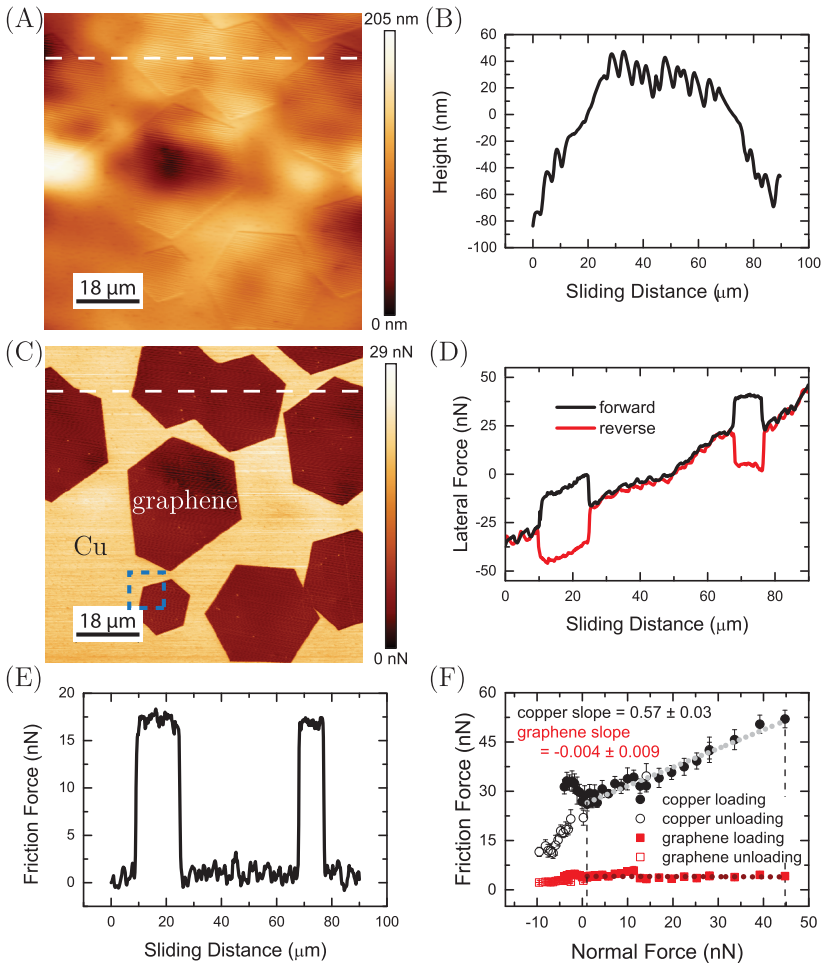

Figure 1. Simultaneously acquired 90 × 90 μm^2 (A) topographic and (C) friction force images of the surface of the copper foil partially covered by graphene islands, obtained at a normal force of −3.2 nN. Height scales are indicated on the right of (A) and (C) for each image. Low (high) friction areas correspond to graphene (oxidized Cu). (B) Topographic and (D) lateral force line profile along the white dashed line marked in (A) and (C), respectively. The overall positive slope in the lateral force profile is an artifact due to the curvature of the copper foil. (E) Friction force profile along the same line shows that graphene reduces friction by a factor of 17 compared to Cu at this load. (F) Friction force *versus* load plot for graphene and copper acquired in a single region spanning the graphene-Cu boundary (indicated by the blue square in (C)). The slopes from fits of the linear portions of the data for graphene and copper are shown with a dashed dark red and gray line, respectively. The vertical black dashed lines indicate the range over which the fit was conducted. Error bars represent the standard deviation in the mean normal and friction forces. The scan speed for (A−E) was 90 μm/s, and for (F) it was 15 μm/s.

the formation of a low density oxide on the uncovered copper surface after removing the sample from the CVD furnace, while the copper underneath the graphene is protected from oxidation[26] (for convenience, we will refer to the exposed, oxidized copper surface as copper throughout this paper). This makes the determination of the location and the thickness of the graphene islands nearly impossible from topographic imaging.

The friction difference between graphene and copper observed in Figure 1(C) can be quantified in lateral force and friction force profiles in Figure 1(D,E), respectively. The overall tilting of the lateral force loop in Figure 1(D) is a result of the irregular and curved topography of the copper foils, which causes a local, slope-dependent offset to the lateral force, and is inconsequential to the determination of friction forces since the effect largely cancels when forward and reverse lateral force data are subtracted.[27]

The friction force image in Figure 1(C) shows that the graphene islands are of extremely high quality: there are, apparently, limited numbers of defects within an individual graphene island, which is evident by the homogeneity of the friction force within a single graphene island. Optical and Raman spectroscopy measurements are shown in the Supporting Information (Figure S1(A,B) respectively), confirming the presence of single graphene layers with a low defect density. However, there are variations in the friction force, which can be seen in the friction force line profile (Figure 1(E)) and the topography line profile (Figure 1(B)), which are larger than variations seen on the copper substrate. This is seen much more clearly at higher magnification and is not simply random in nature, as we discuss below.

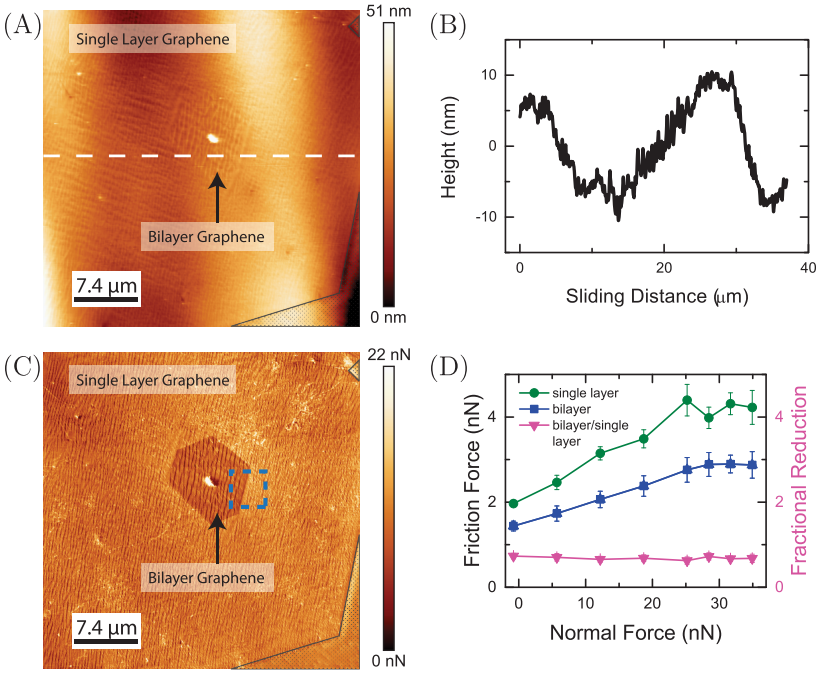

Figure 2. (A) 37 × 37 μm^2 topographic image of a single layer graphene island with a second layer graphene island growing at the center of the image, and the accompanying line profile (B) taken from the region marked by the white dashed line in (A). The boundary between the copper and single graphene layers have been marked with black lines, and the copper area shaded with a black dotted pattern. (C) Friction force image (normal force = 5 nN) of the same area shown in (A). Friction images clearly identify bilayer regions from single layer regions of graphene. (D) Friction force as a function of normal force between the first and second layer of graphene. The region where this load dependence measurement was taken is marked by the blue square in (C). Error bars represent the standard deviation in the mean normal and friction forces. The fractional reduction (the friction force measured on bilayer graphene divided by the friction measured on single-layer graphene) in friction (pink) at each normal load is also plotted in (D), indicating a 68% reduction in friction from one layer to two layers of graphene. The deposition temperature of this sample was 1040 ± 1 °C. The scan speed for images (A), (C), and (D) was 74 μm/s, and for (D) the scan speed was 72.8 μm/s.

Figure 1(F) shows a typical example of the variation of the friction force with normal force. For this data, the tip was scanned over a region containing both graphene and the Cu substrate in each line (10 μm), thus tip changes are not responsible for the observed differences. The normal load dependence of friction was measured with both increasing and decreasing load, to observe if any irreversible processes, such as wear or hysteretic deformation of graphene, occurred during the friction measurement. No significant hysteresis in the loading and unloading data acquired on either graphene or copper is observed at applied positive (compressive) loads, with no effects similar to those reported in Deng *et al.* observed, such as a negative differential friction coefficient measured upon unloading.[12] Several other measurements over a graphene−copper boundary have reproduced an overlapping (nonhysteretic) loading and unloading dependence of friction on normal force, and are shown in Figure S2 in the Supporting Information. The modest hysteresis between the loading and unloading friction forces measured at normal forces less than 0 nN in Figure 1(F) is likely result of contaminants on the surface, causing increased friction during the loading portion. This effect was occasional, *i.e.*, was not observed in most other load dependence measurements (see Supporting Information). We see no evidence of damage to the sample by scanning. The friction behavior was repeatable in all cases, and we observed no change in the topography or the friction response even after several hours of multiple scans over the same region of the sample. A linear fit to the friction *versus* normal force data in the linear portion of the data in Figure 1(F) (from 1 to 45 nN) produced slopes of 0.57 ± 0.03 on copper and −0.004 ± 0.009 (statistically indistinguishable from zero) on graphene. Friction *versus* load measurements performed with other AFM tips on this sample exhibited a similarly reduced slope for graphene compared with copper, but the friction *versus* load slopes could have values that were statistically distinct from zero (see Supporting Information). Note that any sliding history dependent phenomena, such as the creation of a pucker,[8] can be lost each time the tip slides across the graphene−copper boundary.

Frictional Behavior of Bilayer Graphene. In some regions, a second layer of graphene has nucleated and grown near the center of a monolayer island. This occurrence is very infrequent: optical microscopy imaging of the sample shows that over square centimeter regions, typically only 2−3 graphene islands contain a second layer. The second layer of graphene is known to grow beneath the first layer.[28−30] Figure 2(A) shows a

topographic image of an area of the copper foil containing both a single and a double layer of graphene. The small feature in the center of the second layer of graphene is a contaminant particle, with a height of approximately 40 nm. These contamination particles have been shown to act as nucleation sites for graphene deposition on copper foils.[31,32] With this topographic data, it is impossible to determine the thickness (*i.e.*, number of layers) of the graphene sheet or if this contaminant particle is above or below the graphene sheets. To further demonstrate the difficulty in using topographic data to determine the graphene thickness, a topographic line profile indicated by the dashed white line in Figure 2(A) is shown in Figure 2(B). Similar to the results in Figure 1, topographic imaging cannot be used to easily identify the thickness of graphene layers, primarily because of the underlying topographic undulations of the copper foil. Similar observations of subsurface second layer graphene islands grown on copper surfaces have been demonstrated[30,33] and have a similar appearance to the second layer of graphene shown in Figure 2(A).

Figure 2(C) shows a friction force image of the same area. With this friction data, it now becomes clear that a second layer of graphene is present in the area surrounding the contaminant particle. Figure 2(D) shows the variation of the friction force with increasing normal force acquired in the area indicated by the dashed blue box in Figure 2(C). At every load, friction on the second layer of graphene is lower than on the single layer, showing an average 67 $\pm$ 3% decrease in friction from one to two layers of graphene. This result of Figure 2 for CVD-grown graphene is consistent with previous results of friction properties of multilayer graphene sheets produced through mechanical exfoliation and thermal decomposition.[7,8] Friction contrast in the lower right region between copper and the single graphene layer is lower in comparison to Figure 1(C) because of a much longer exposure time to the laboratory environment of several months in the case of Figure 2(C), compared to hours in Figure 1(C).

Wrinkles in Graphene Sheets. Figure 3(A) was acquired on the same sample shown in Figure 1. This island corresponds to the island marked with the blue dotted square in Figure 1(C). As previously discussed, the topographic image shown in Figure 3(A) cannot be used to identify the height of the graphene surface, resulting from the overall roughness of the copper substrate. The topographic image does show that there are wrinkles in the graphene island, and that the graphene island is slightly depressed in height compared to the surrounding surface. Both are clearly evident in the topographic line profile shown in the inset of Figure 3(A), taken along the white dashed line. The line profile shows that the wrinkle amplitude is approximately 15 nm. Once again, the observed depression of the graphene sheet relative to the copper substrate is a result of the formation of an oxide film on the copper substrate following graphene deposition. This obscures the height measurement, which makes graphene thickness determination under ambient conditions impossible.

Figure 3(B) shows a friction force image of the same area. Figure 3(B) also shows that the friction force is modulated by the wrinkled structure of the graphene island, in contrast to any observed wrinkling in the friction force outside of the graphene island. As shown in the lower magnification image in Figure 3(B), the graphene island is continuous and of high quality, except for a few regions of high friction that are believed to be contaminants on the copper surface during deposition. These contaminants, again, are almost impossible to identify in topographic images of the surface, as evident by Figure 3(A), but are readily observed in the friction force image (Figure 3(B)) as localized areas of increased friction surrounded by a low friction area within a graphene island. Although the presence of wrinkles in the graphene sheet is consistent with previous reports,[17,22,34] wrinkles with the regularity observed in these Figure 3(A,C) have not been previously observed. Choi *et al.* proposed that exfoliated graphene samples they examined possessed ripples that led to anisotropic friction. We do not observe such effects in these CVD samples, nor do we observe friction anisotropy. The formation of the wrinkles in graphene islands is most often proposed to be the result of the different coefficients of thermal expansion of graphene and copper leading to a compressive strain in the graphene upon cooling after growth,[17,35] but may also be a result of faceting of the copper surface along certain crystallographic planes to produce terraces separated by step bunches, giving a "zig-zag" surface topography.[36]

Figure 3(C) shows a different island located on a different sample that shows the same variation of the surface topography over a small region. In this image, the sample has been rotated so that the wrinkles were oriented 90° to the fast scan (horizontal) direction, to obtain a more accurate measurement of the wrinkle amplitude (topographic measurements are more accurate along the fast-scan direction since drift and $1/f$ noise are minimized). The wrinkle amplitude, or the variation of the measured topography within a graphene island when measured perpendicular to the wrinkles, is in the range of 10−25 nm as shown by the topographic line profile in the inset of Figure 3(C), obtained along the white dashed line. Figure 3(D) shows the friction contrast measured when scanning on the graphene island shown from Figure 3(A), measured within the region marked by the blue dashed square. There are several lines showing bright (positive) contrast against the background, the brightest of which have been marked by black arrows. These lines reflect the underlying copper steps of the foil, as graphene is known to grow continuously over copper

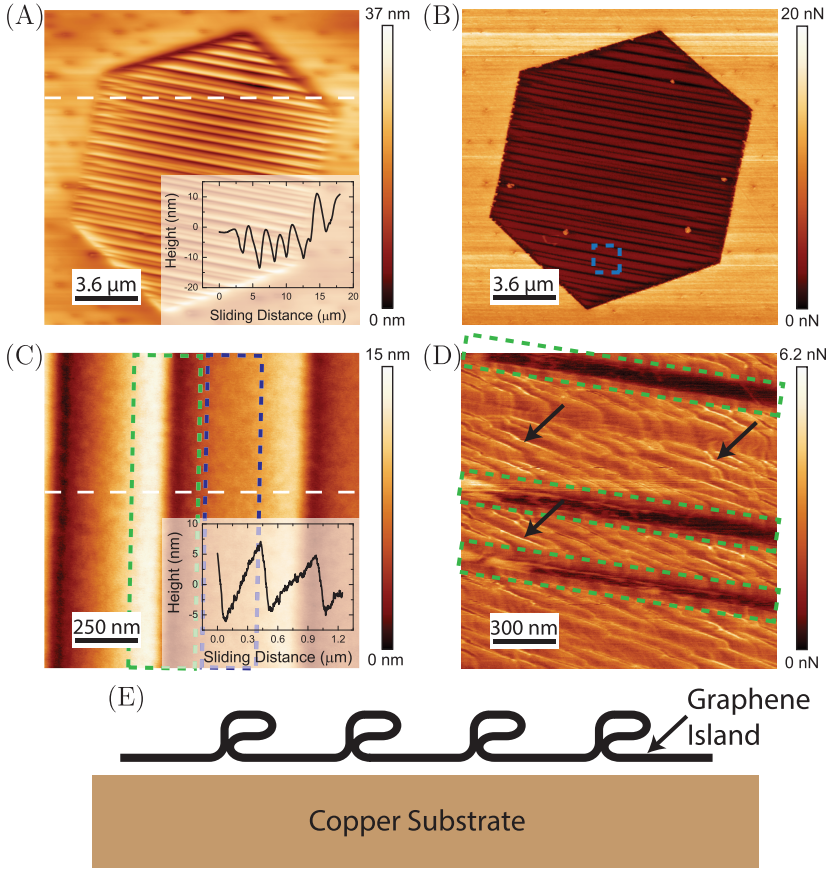

Figure 3. (A) Topographic image of a single graphene island on copper (18 × 18 μm^2). A white dashed line marks the line along which the topographic line profile shown in the inset of (A) is taken. (B) Friction force image (normal force = 6.5 nN, scan speed = 50 μm/s) of the same area in (A). The light blue dashed box indicates the area shown in (D). (C) Topographic image acquired on a graphene island (scan size = 1.2 × 1.2 μm^2). The green and dark blue dashed boxes show the two regions of the graphene sheet, the wrinkle edge, and the flat graphene sheet. The inset shows a topographic line profile taken along the white dashed line showing that the typical height variation on the graphene surface is 15 nm. (D) Friction force image of the same graphene island in (A) and (B) showing a variation of friction over the wrinkled surface (scan size = 1.5 × 1.5 μm^2, normal force = 11 nN, scan speed = 15 μm/s). Similarly, green dashed boxes highlight the wrinkled area, as in (C). Black arrows point to the lighter contrast features, believed to be copper step edges beneath the graphene island. (E) Schematic of the proposed structure of the wrinkles within the graphene island.

steps during the CVD growth process.[21] The occurrence of these steps and the absence of a large change in topography over a single graphene island suggest that the copper beneath the island is a region of single crystalline copper. Also visible in Figure 3(D) are several parallel bands of darker contrast, approximately 30−100 nm in width and contained within green dashed boxes shown on the figure. These bands occur at the same location as a wrinkle edge, *i.e.*, the point where the topography is the highest for each wrinkle (also marked on Figure 3(C) with a green dashed square). These features have a very large width (typically ∼20−100 nm) compared with the tip radius (assumed to be between 10 and 15 nm). The size difference between the tip and the observed area of low friction strongly suggests that the area of low friction is not an artifact from imaging the surface. Furthermore, the underlying copper steps cannot be observed in these bands, but reappear on the other side of one of these dark bands. Given the structure of these wrinkles proposed in the literature,[22] the decreased friction in the region of the wrinkle edges may be a result of multilayer graphene *versus* single layer graphene, formed by a "fold-over" structure,[7,8] as depicted in Figure 3(E).

The dependence of friction on normal force on the flat graphene sheet, *i.e.*, the region marked by the blue dashed box in Figure 3(C), was investigated; the result is summarized in Figure 4. Specifically, the friction *versus* load dependence is taken from only the graphene sheet (marked by the blue dashed box in Figure 3(C)). Two friction *versus* load measurements were taken in this specific location and are shown in Figure 4. In each measurement, the tip was initially out-of-contact with the surface, brought into contact with the surface, the load gradually increased to a maximum value, and then unloaded at the same rate until the pull-off point, resulting in a loss of contact between the sample and tip. The first friction *versus* load measurement is colored blue, and the second is teal. In the first measurement (test 1, blue data points), the maximum

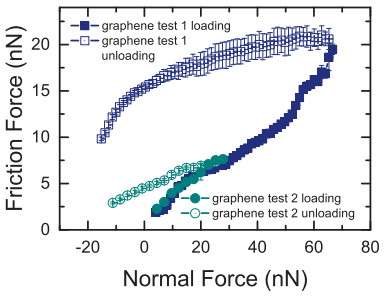

Figure 4. Load dependence of friction on unwrinkled areas for a monolayer island. The maximum normal load is 66 nN in test 1 and 27 nN in in test 2 using the same tip on the same area. The higher applied normal load in test 1 results in larger hysteresis between loading and unloading compared to test 2. Error bars represent the standard deviation in the mean normal and friction forces measured. Test 1 and 2 were acquired at a scan speed of 13 μm/s and 10.4 μm/s, respectively. Load dependence data taken from the regions marked by the blue dashed rectangles in Figure 3(B).

normal force was 66 nN. In this curve, the loading and unloading curves do not overlap. More specifically, the friction at each normal load is higher during unloading compared loading. In the subsequent section, the mechanism explaining this hysteresis will be explored. However, the primary difference to explain this observed hysteresis results from the fact that contact with the graphene sheet and the tip has not been broken at any point during the load dependence measurements shown in Figure 4, unlike when scanning over the boundary between copper and graphene. In the latter case, contact between the tip and the graphene sheet is lost every time the tip crosses the boundary. Figure 4 shows another measurement (test 2, teal data points) showing the same type measurement, where the maximum load was 27 nN. In this case, the difference between loading and unloading in the variation of friction force with normal force is much lower. In both cases, this observed hysteresis is not an effect of sample wear, as examination of the surface following these measurements did not reveal any alteration of the surface features. Furthermore, the lateral spatial resolution in the lateral force images did not change during the load dependence measurement or in any other repeated measurements not included within this paper, indicating that tip wear is also not responsible for the observed hysteresis. Finally, the two loading curves acquired in each test overlap perfectly, suggesting the same tip size and interaction between the tip and sample during each measurement. Only one such measurement, *i.e.*, when the same tip used to measure the normal force dependence of friction at the same spot on the sample, was performed. However, in two other measurements with two different tips, the graphene friction measured similar to Figure 1(D) (*i.e.*, crossing over the boundary from oxidized copper to graphene, and measured during loading as in Figure 4, *i.e.*, graphene friction measured on a single island) also overlapped, further indicating an absence of tip wear during these measurements. These two examples are included in the Supporting Information. We propose that a combination of the "pucker effect" observed on atomically thin film materials that are weakly bound to a substrate[8] and local layer delamination[12] is responsible for the observed hysteresis in the friction force *versus* normal force measurements, as described further in the next section.

The Pucker Effect and Layer Delamination. The following section will be primarily devoted to understanding the load dependence of friction observed while scanning on an individual, mechanically exfoliated flake of graphene, and how it contrasts with the load dependence of friction measured while scanning over a graphene–copper boundary for CVD-grown graphene on copper.

In a recent study by Lee *et al.*, it was suggested that low dimensional materials can develop an increased contact area with the tip by the formation of a pucker in the thin film that forms in front of a contacting, sliding tip.[8] This pucker results from the low out-of-plane bending stiffness of thin films compared the stretching modulus of the atomically thin sheet. The formation of a pucker in front of the sliding tip is dependent on a low work of adhesion between the graphene sheets and the supporting substrate, allowing the graphene to partially debond from the substrate and interact adhesively with the tip. The strength of this pucker was shown to depend on the adhesion of the thin film to the substrate. The increased contact area between the tip and the thin film then increases friction. The ability to form the pucker depends on the out-of-plane bending stiffness of the atomic sheet; the sample's flexural stiffness increases rapidly with increasing numbers of layers. Therefore, friction increases markedly as the number of sheets reduces to one layer, as long as the sheet is not strongly adhered to the substrate. Strong adhesion to the substrate inhibits the out-of-plane deformation, and the friction behavior then remains similar to that of the bulk structure. Recent molecular dynamics (MD) simulations confirmed the effect of puckered graphene on friction, and found that the degree the pucker affects friction is also dependent on the size of the graphene flake in multilayer graphene;[11] however, the graphene islands discussed in this paper are much larger than the identified minimum required to support enhanced friction through puckering. The layer-dependent friction observed on CVD grown graphene on polycrystalline copper is consistent with the literature reporting enhanced friction through the formation of a pucker.

The formation of a pucker requires not only a low out-of-plane bending stiffness for graphene, but also low graphene-substrate adhesion in comparison to tip-graphene adhesion.[8] Furthermore, sliding history-dependent friction requires enhanced adhesive forces between the graphene and the tip, compared to the

graphene and the substrate.[12,37] The work of adhesion between graphene and copper has been determined by a macroscopic fracture mechanics method for low temperature CVD-grown graphene on copper (~725 °C deposition temperature) to be 0.72 J/m^2.[38] The work of adhesion between silicon AFM tips and exfoliated graphene has been determined to be 0.23 J/m^2.[37] The larger work of adhesion between copper and graphene than between the AFM tip and graphene suggests that sliding history-dependent friction should not occur. However, several reports have shown that the copper−graphene adhesive properties in CVD-grown graphene are influenced by a number of factors, including crystallinity of the copper surface[21] and the presence of dislocations near the surface of copper.[20] Additionally, the presence of wrinkles, similar to those observed in Figure 3, are proposed to result from a loss in crystallinity of the copper substrate beneath the graphene island.[17] We therefore hypothesize that the adhesive interaction between the copper substrate and the graphene film must be lower than 0.72 J/m^2 because of a loss of crystallinity in the copper substrate below the graphene islands. This lowered adhesive interaction between copper and graphene enables the formation of a pucker in the graphene film, as well as sliding history-dependent friction.

The difference in load dependence curve between single and bilayer graphene observed in Figure 2 is similar to previously reported results,[7,8,39] as discussed earlier. The mechanism for the layer dependence of friction has been explained through a change in electron−phonon coupling between the graphene layer and the substrate,[7] and through the pucker effect.[8] However, the hysteresis between the loading and unloading friction data shown in Figure 4 and the low adhesion between the copper and graphene that is typically found in similarly prepared CVD samples suggests that the pucker effect is the likely mechanism for the layer dependent friction.

Reversible loading and unloading curves (*i.e.*, when the two curves are indistinguishable) indicate the same contact and friction forces exist as the load is increased compared to when the load is decreased, as shown in the literature.[12,40,41] In contrast to the result in Figure 4, when wear of the surface[41] (or tip) changes the interaction strength/size between the tip and the surface, or when the interaction forces between the tip and the substrate change resulting from a sliding-induced phenomena,[12] the loading and unloading friction curves do not overlap. The completely overlapping loading curves in Figure 4 indicate that no wear of the tip/surface has occurred between the two measurements, and that the interaction forces between the tip and sample are not changing with time. As noted previously, the contact between sample and tip had been broken and re-established many times between these measurements.

In contrast to the loading curves from the two friction measurements in Figure 4, the loading and unloading curves from a single measurement do not overlap: the friction measured during loading is significantly lower than what is measured during unloading. The overlapping friction *versus* normal force curve for the two loading measurements in Figure 4 prove that the tip and sample wear are not occurring, and therefore wear is not responsible for the observed hysteretic behavior and that a more complex phenomena must be responsible.

It has recently been shown that graphene, when exposed to an oxidizing environment, can develop stronger adhesive properties between the tip and the topmost graphene layer, than between the substrate or other graphene layers.[12,37] This increased adhesion can give the topmost layer the ability to stick to the tip and debond locally around the tip during friction measurements. Furthermore, in contacts where topmost layer of graphene is more adhesive to the tip than the substrate, the adhesive strength between the tip and the sample depends on the sliding-history of the contact: *i.e.*, the degree of adhesive interaction, and thus the measured pull-off force, between the tip and topmost layer of graphene increases with sliding distance.[37] This additional information can now aid the interpretation of the friction measurements that have shown seemingly opposing results: when scanning over a copper/graphene boundary interface or between successive friction measurements performed on graphene, no hysteresis is observed compared to the large hysteresis recorded between the loading and unloading curves obtained while sliding on a single graphene sheet.

During a friction *versus* normal force measurement, such as the one conducted in Figure 4, no loss of contact between the graphene and tip occurs between the loading and unloading measurements. Similarly in other friction *versus* normal force measurements, such as in Figure 1(D), the contact between the surface and the tip is not broken when transitioning from loading to unloading. However, in measurements across the copper−graphene boundary, such as in Figure 1(D), the tip loses contact with the graphene film each time the tip traverses the boundary. This difference between the two measurements now can be used to identify situations where a sliding-history dependent friction occurs.

The following mechanism for the observed hysteresis in the load dependence curves is proposed and illustrated in Figure 5. Initially, the tip is out of contact with the sample. Upon approaching the tip to the surface (Figure 5(A)), the graphene sheet deforms symmetrically beneath the tip because of the adhesive and compressive forces that exist between the tip and the sample. As the tip slides in the plane of the surface, the low out-of-plane stiffness results in the formation of a pucker (Figure 5(B)), or a small bump in the

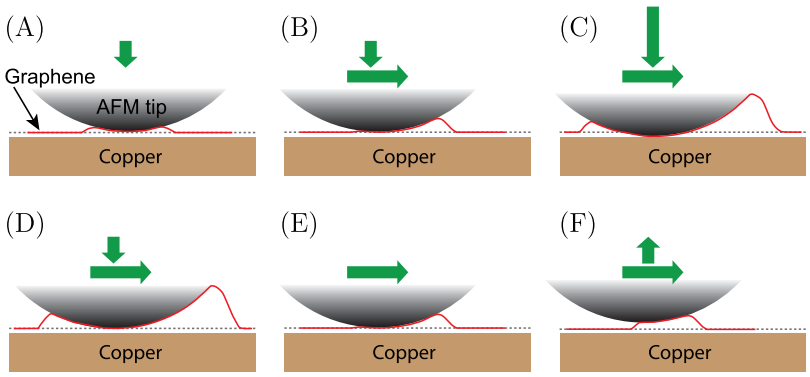

Figure 5. Schematic of the structure of the graphene sheet (red solid line) supported by a copper substrate at various stages of a typical load dependence measurement. A gray dashed line indicates the shape of the graphene sheet in the absence of the tip. (A) The structure of the graphene sheet upon first contact with the tip before any sliding has occurred. (B) As the tip begins to slide, a pucker is created in front of the sliding tip. (C) As the normal force increases, so does the height of the pucker. (D) When the normal force is decreased after reaching a maximum value, the high adhesion between the graphene sheet and the tip does prevents a decrease in the size of the pucker at the same rate as it was built up. At zero applied load (E) and adhesive loads (F), a pucker is still observed in the graphene sheet. The magnitude of the normal force is shown by the vertical green arrows above the gray tip. Horizontal green arrows indicate the direction of sliding of the tip.

graphene sheet in front of the sliding tip, at compressive loads. The influence of a pucker on friction has been well documented in Liu *et al.*:[37] the primary effect of the out of plane deformation of the graphene sheet is that an increase in contact area between the tip and the graphene sheet is observed, when compared to what would be expected if the graphene was a rigid body that does not form a pucker. As the normal force increases, so does the size of the pucker until a maximum normal force has been reached (Figure 5(C)).

Then, as the loading direction is reversed, the substantial adhesive force between the tip and the surface, resulting from the oxidation of the graphene sheet,[12] inhibits the graphene sheet from fully relaxing (Figure 5(D)). Therefore, the structure of the graphene sheet is not reversible during unloading. In other words, during unloading, the puckered structure only partially relaxes; *i.e.*, it does not recover the size it had been when increasing the normal force (Figure 5(E,F)). The hysteresis between the loading and unloading curves suggests that the rate of decrease of the size of the pucker occurs much more slowly than the rate it increased with normal force. The formation of a larger contact area with the graphene sheet (assuming the graphene sheet did not form a pucker) and the buildup of the pucker in front of the sliding tip are indistinguishable if only measured in the loading or unloading directions. However, since both loading and unloading measurements were acquired, we can distinguish between these two mechanisms. Evidence of the increased adhesion between the tip and the surface resulting from oxidation of the graphene sheet is demonstrated by the slower rate of decrease of the friction force during unloading compared to loading. Since the tip and the surface remain unchanging, the hysteresis between loading and unloading results from a difference in contact area between the tip and the surface at the same normal forces.

Comparison between test 1 and test 2 in Figure 4 suggest that the formation of the pucker in front of the sliding tip is load dependent, as the hysteresis in the unloading and loading friction force is much greater when for higher maximum loads.

Importantly, during these measurements, the AFM tip was continually scanned without separating the tip and the sample and was always scanning over graphene (*i.e.*, not traversing an area of copper). Separating the tip from the sample destroys any previously formed pucker in front of the tip, as we can show through the two consecutive load dependence of friction measurements. The sliding-induced development of enhanced contact area is also consistent with recent studies of adhesion measurements between AFM tips and graphene samples:[37] the pull-off force measured when the tip has been previously scanned across graphene without any separation is higher than that measured when no scanning has occurred.

Furthermore, the load dependence of friction shown in Figure 1(D) and Figure S2(D−F) (Supporting Information) show no hysteresis. In these measurements, in each line the tip was slid over both a graphene region and an exposed copper region. Breaking contact between the tip and the graphene allows the local deformation of the graphene to relax. Thus, we propose that the friction force between the tip and graphene depends substantially on the sliding history, because of the transient deformability of the graphene around the tip. This deformed configuration is mobile and remains localized around the tip as it scans, but it rapidly relaxes when the tip is no longer in contact with the graphene. This suggests that reducing and/or predictably controlling friction against graphene requires constraining the graphene strongly to the substrate and minimizing adhesion between the graphene and the sliding asperity.

CONCLUSIONS

The frictional properties of CVD graphene grown on copper polycrystalline foils have been investigated. The load dependence of friction shows that graphene lowers the friction experienced by an AFM tip substantially compared to the surrounding oxidized copper surface by a factor of 1.5−7. Load dependence measurements made on samples where graphene was deposited at various temperatures shows that, while the island shape is significantly affected, the apparent quality of the graphene, as indicated by the uniformity of the friction force within an island, is not affected by the deposition temperature, when compared to the reference oxidized copper surface. Load dependence measurements show that bilayer graphene exhibits lower friction than single layer graphene at all loads, consistent with measurements on exfoliated[8] and thermally grown[7] graphene. The load dependence of friction on graphene depended strongly on the sliding history. If measurements are acquired so that the tip breaks contact with the graphene (by crossing the copper−graphene edge), no hysteresis between loading and unloading measurements was observed, whereas a significant hysteresis was observed in load dependence measurements obtained solely on the graphene sheet. We propose that the hysteresis is a result of the formation of a puckered deformation in front of the sliding tip during scanning, whose size is dependent on the normal force applied and the sliding history. The observation of layer dependent friction and hysteresis in the load dependence suggest that the graphene sheet is weakly bound to the underlying copper substrate compared to its adhesive interaction with the tip. The layer-dependent friction in CVD grown graphene observed is more consistent with the thin film puckering mechanism,[8] rather than enhanced electron phonon coupling.[7] Minimizing and predicting friction of asperities against graphene can be achieved by (1) increasing the adhesive interaction between graphene and the substrate it is supported on; (2) reducing adhesion of the graphene to the tip; and (3) using multilayer, not single layer graphene.

METHODS

Graphene Synthesis. Copper foils with a thickness of 25 μm were purchased from Alfa Aesar, Inc., and cut into square pieces of approximately 5 cm × 5 cm. Immediately before graphene growth, the copper foils were gently sonicated in acetic acid for 5 min (12 W, 10 min) to remove the native oxide layer and other contamination on the foil surfaces. Following sonication, the copper foils were rinsed with deionized water and placed on a flat alumina surface, inserted into a vacuum furnace, and annealed at 1050 °C for 1 h to increase the grain size in the copper foil, as well as to remove residual strain in the foil. This annealing process also reduced the RMS roughness of the surface and reduced the density of potential graphene growth nucleation sites on the surface,[24] and was confirmed by topographic measurements of the foil before and after this step. During annealing, the furnace was evacuated and subsequently filled with 5 ccm of argon and 200 ccm of hydrogen (to a pressure of 1 atm) to prevent the formation of an oxide during annealing. Furthermore, the presence of hydrogen during this annealing stage has been shown to further reduce the roughness of copper foils.[42] After this annealing stage and subsequently cooling the sample back to room temperature, the sample was further etched with CE100 etchant (Transene Company, Inc.) by wiping the copper foil with a kimwipe dampened with the etchant for approximately 5 s. Following this polishing step, the copper foil was rinsed with deionized water.

The resulting growth of hexagonal-shaped islands, as well as quality and layer thickness assessed using Raman spectroscopy, is described in the literature.[24] Briefly, the graphene island growth was performed at atmospheric pressure. The foils were placed in a furnace with a controlled atmosphere of Ar (500 sccm) and H_2 (50 sccm), and then heated to 1057 °C, unless otherwise noted. Once this temperature was reached, the flow rate of H_2 was reduced to 35 sccm, and a flow of CH_4 (2 sccm) was introduced and maintained for 30 min. The effect of deposition temperature on the quality of graphene sheets produced was investigated by using two other deposition temperatures, 1040 and 1020 °C. Following deposition, the sample was quenched to room temperature. After a further 10 min, the CH_4 gas flow was suspended, and the sample was removed from the deposition chamber; at this point the sample temperature was below 100 °C. In all cases where friction on graphene is compared with copper, the surfaces were examined within 1−4 days of graphene growth. Samples examined after much longer periods show a large amount of carbon present on the surface, despite being stored in dry nitrogen. Also, as samples are examined in ambient conditions, we assume that the copper surface not covered by graphene is indeed oxidized.

Friction Experiments. An Asylum Research MFP-3D beam deflection atomic force microscope (AFM) was used for all friction measurements. All measurements were conducted at room temperature (~21 °C) under ambient conditions (room humidity ~30−50%). The outer 0.5 mm of the copper foils were attached to glass slides with double-sided tape to provide extra mechanical stability during scanning. These attachment of the copper foils was performed with care taken to prevent any mechanical deformation of the coper foils.

Silicon cantilevers with an integrated tip (PPP-CONT, Nanosensors) that terminates with a native silicon oxide were used in all experiments. The normal and lateral spring constants of these cantilevers are typically between 0.05 and 0.1 N/m and between 30 and 100 N/m, respectively. The individual stiffness of each of the cantilevers in both normal bending and lateral twisting was calibrated by measuring and fitting the thermal resonance of the first normal mode in both normal bending and lateral twisting signals to obtain the respective frequencies and *Q*-factors. These parameters, along with the plan view dimensions of the cantilever (*i.e.*, the length and the width of the cantilever beam) were then used to determine the spring constants using the Sader method.[43,44] The sensitivity of the photodetector, allowing for the conversion of photodetector signal volts to nanometers, was determined by measuring the slope of the cantilever deflection signal in a normal force−distance curve. The lateral sensitivity of the quadrant detector was assumed to be the same as the sensitivity measured in the normal bending direction. We define zero normal force as the signal measured when the cantilever is unbent and far from the surface. Therefore, compressive forces are recorded as positive normal forces and tensile forces as negative normal forces. Lateral forces corresponding to the twisting signal were measured during scanning. Friction forces are then the average of the difference between the lateral forces measured during sliding in the forward and reverse directions. The fractional reduction of friction is defined as the friction force measured on bilayer graphene surfaces divided by the friction

force measured on single-layer graphene. All results have been reproduced with multiple tips and multiple graphene regions to verify consistent trends. Furthermore, in all load dependence measurements where a heterogeneous surface is examined (*e.g.*, comparing graphene with surrounding copper), data were acquired by scanning the tip across the boundary of the two materials, ensuring the contrast revealed is not due to changes of the tip.

All friction *versus* normal force measurements were taken in both loading and unloading directions, with the exception of the results shown in Figure 2(B), which were acquired in the unloading direction only. To acquire the friction data, the following procedure was used: (1) A normal force *versus* distance curve was acquired to determine the initial zero deflection or normal force value. (2) The tip was brought into contact with the sample, and friction forces were measured starting at a value of the normal force roughly corresponding to this initial zero deflection (*i.e.*, zero externally applied load), and then subsequently increasing the normal force by small, defined increments after the completion of a single scan/image, until a maximum, predetermined value of the normal force was reached. Friction acquired in this manner (*i.e.*, with increasing load) is referred to as friction acquired during loading. (3) After the maximum normal force was reached, the normal force was then incrementally decreased until the tip pulled out of contact from the surface. Friction measured in this way is referred to in the manuscript as friction acquired during unloading. (4) A force *versus* distance curve was acquired following the friction measurement to determine the zero deflection value. This value was then used to determine the amount of drift in the zero position of the normal force that occurred during the measurement. This drift was accounted for by assuming the drift changed linearly during the measurement, and either added or subtracted from the initial zero deflection value for each data point shown in the load dependence measurement. The sliding speed for each measurement is reported in the figure captions. AFM images were analyzed with the WSXM software.[45] In all friction force images presented, darker (brighter) color indicates lower (higher) measured friction forces.

Conflict of Interest: The authors declare no competing financial interest.

Acknowledgment. This work was supported by the National Science Foundation (NSF) under Awards NSF/MRSEC (No. DMR11-20901) & NSF/ENG (CMMI-1068741). Use of University of Pennsylvania Nano/Bio Interface Center instrumentation is acknowledged, which is funded through NSF Grants No. NSEC DMR08-32802, DBI-0721913, and DMR-0425780. The optical micrograph and Raman spectroscopy data in the Supporting Information were collected by Sung Ju Hong, Prof. Yung Woo Park research group at Seoul National University. P. Egberts would like to acknowledge financial support from the Natural Sciences and Engineering Council (NSERC) of Canada. Also, the support in creating the analysis scripts from Joel Lefever and James Hilbert as well as insightful discussions with Dr. Graham Wabiszewski are acknowledged. G. H. Han and A. T. C. Johnson acknowledge support from the Nano/Bio Interface Center, NSF Grant No. NSEC DMR08-32802.

Supporting Information Available: Optical images with corresponding Raman spectroscopic data of graphene samples transferred onto silicon, as well as friction data acquired on three graphene samples on the copper foil, whose deposition temperature was varied from 1020 to 1057 °C. This material is available free of charge *via* the Internet at http://pubs.acs.org/.

REFERENCES AND NOTES

1. Li, X.; Cai, W.; An, J.; Kim, S.; Nah, J.; Yang, D.; Piner, R.; Velamakanni, A.; Jung, I.; Tutuc, E.; *et al.* Large-Area Synthesis of High-Quality and Uniform Graphene Films on Copper Foils. *Science* **2009**, *324*, 1312–1314.
2. Bae, S.; Kim, H.; Lee, Y.; Xu, X.; Park, J.-S.; Zheng, Y.; Balakrishnan, J.; Lei, T.; Kim, H. R.; Song, Y. I.; *et al.* Roll-to-Roll Production of 30-Inch Graphene Films for Transparent Electrodes. *Nat. Nanotechnol.* **2010**, *5*, 574–578.
3. Lee, G.-H.; Cooper, R. C.; An, S. J.; Lee, S.; van der Zande, A.; Petrone, N.; Hammerberg, A. G.; Lee, C.; Crawford, B.; Oliver, W.; *et al.* High-Strength Chemical-Vapor-Deposited Graphene and Grain Boundaries. *Science* **2013**, *340*, 1073–1076.
4. Novoselov, K. S.; Geim, A. K.; Morozov, S. V.; Jiang, D.; Zhang, Y.; Dubonos, S. V.; Grigorieva, I. V.; Firsov, A. A. Electric Field Effect in Atomically Thin Carbon Films. *Science* **2004**, *306*, 666–669.
5. Berger, C.; Song, Z.; Li, X.; Wu, X.; Brown, N.; Naud, C.; Mayou, D.; Li, T.; Hass, J.; Marchenkov, A. N.; *et al.* Electronic Confinement and Coherence in Patterned Epitaxial Graphene. *Science* **2006**, *312*, 1191–1196.
6. Lee, C.; Wei, X.; Kysar, J. W.; Hone, J. Measurement of the Elastic Properties and Intrinsic Strength of Monolayer Graphene. *Science* **2008**, *321*, 385–388.
7. Filleter, T.; McChesney, J.; Bostwick, A.; Rotenberg, E.; Emtsev, K.; Seyller, T.; Horn, K.; Bennewitz, R. Friction and Dissipation in Epitaxial Graphene Films. *Phys. Rev. Lett.* **2009**, *102*, 086102.
8. Lee, C.; Li, Q.; Kalb, W.; Liu, X.-Z.; Berger, H.; Carpick, R. W.; Hone, J. Frictional Characteristics of Atomically Thin Sheets. *Science* **2010**, *328*, 76–80.
9. Shin, Y. J.; Stromberg, R.; Nay, R.; Huang, H.; Wee, A. T.; Yang, H.; Bhatia, C. S. Frictional Characteristics of Exfoliated and Epitaxial Graphene. *Carbon* **2011**, *49*, 4070–4073.
10. Lui, C. H.; Liu, L.; Mak, K. F.; Flynn, G. W.; Heinz, T. F. Ultraflat Graphene. *Nature* **2009**, *462*, 339–341.
11. Ye, Z.; Tang, C.; Dong, Y.; Martini, A. Role of Wrinkle Height in Friction Variation with Number of Graphene Layers. *J. Appl. Phys.* **2012**, *112*, 116102.
12. Deng, Z.; Smolyanitsky, A.; Li, Q.; Feng, X.-Q.; Cannara, R. J. Adhesion-Dependent Negative Friction Coefficient on Chemically Modified Graphite at the Nanoscale. *Nat. Mater.* **2012**, *11*, 1032–1037.
13. Smolyanitsky, A.; Killgore, J. Anomalous Friction in Suspended Graphene. *Phys. Rev. B: Condens. Matter Mater. Phys.* **2012**, *86*, 125432.
14. Kwon, S.; Ko, J.-H.; Jeon, K.-J.; Kim, Y.-H.; Park, J. Y. Enhanced Nanoscale Friction on Fluorinated Graphene. *Nano Lett.* **2012**, *12*, 6043–6048.
15. Marsden, A. J.; Phillips, M.; Wilson, N. R. Friction Force Microscopy: A Simple Technique for Identifying Graphene on Rough Substrates and Mapping the Orientation of Graphene Grains on Copper. *Nanotechnology* **2013**, *24*, 255704.
16. Kim, K.-S.; Lee, H.-J.; Lee, C.; Lee, S.-K.; Jang, H.; Ahn, J.-H.; Kim, J.-H.; Lee, H.-J. Chemical Vapor Deposition-Grown Graphene: The Thinnest Solid Lubricant. *ACS Nano* **2011**, *5*, 5107–5114.
17. Zhang, Y.; Gao, T.; Gao, Y.; Xie, S.; Ji, Q.; Yan, K.; Peng, H.; Liu, Z. Defect-Like Structures of Graphene on Copper Foils for Strain Relief Investigated by High-Resolution Scanning Tunneling Microscopy. *ACS Nano* **2011**, *5*, 4014–4022.
18. Gao, L.; Guest, J. R.; Guisinger, N. P. Epitaxial Graphene on Cu(111). *Nano Lett.* **2010**, *10*, 3512–3516.
19. Zhao, L.; Rim, K.; Zhou, H.; He, R.; Heinz, T.; Pinczuk, A.; Flynn, G.; Pasupathy, A. Influence of Copper Crystal Surface on the CVD Growth of Large Area Monolayer Graphene. *Solid State Commun.* **2011**, *151*, 509–513.
20. Tian, J.; Cao, H.; Wu, W.; Yu, Q.; Guisinger, N. P.; Chen, Y. P. Graphene Induced Surface Reconstruction of Cu. *Nano Lett.* **2012**, *12*, 3893–3899.
21. Cho, J.; Gao, L.; Tian, J.; Cao, H.; Wu, W.; Yu, Q.; Yitamben, E. N.; Fisher, B.; Guest, J. R.; Chen, Y. P.; *et al.* Atomic-Scale Investigation of Graphene Grown on Cu Foil and the Effects of Thermal Annealing. *ACS Nano* **2011**, *5*, 3607–3613.
22. Robertson, A. W.; Bachmatiuk, A.; Wu, Y. A.; Schäffel, F.; Büchner, B.; Rümmeli, M. H.; Warner, J. H. Structural Distortions in Few-Layer Graphene Creases. *ACS Nano* **2011**, *5*, 9984–9991.
23. Yu, Q.; Jauregui, L. A.; Wu, W.; Colby, R.; Tian, J.; Su, Z.; Cao, H.; Liu, Z.; Pandey, D.; Wei, D.; *et al.* Control and Characterization of Individual Grains and Grain Boundaries in

Graphene Grown by Chemical Vapour Deposition. *Nat. Mater.* **2011**, *10*, 443–449.
24. Luo, Z.; Kim, S.; Kawamoto, N.; Rappe, A. M.; Johnson, A. T. C. Growth Mechanism of Hexagonal-Shape Graphene Flakes with Zigzag Edges. *ACS Nano* **2011**, *5*, 9154–9160.
25. Ferrari, A. C.; Meyer, J. C.; Scardaci, V.; Casiraghi, C.; Lazzeri, M.; Mauri, F.; Piscanec, S.; Jiang, D.; Novoselov, K. S.; Roth, S.; *et al.* Raman Spectrum of Graphene and Graphene Layers. *Phys. Rev. Lett.* **2006**, *97*, 187401.
26. Schriver, M.; Regan, W.; Gannett, W. J.; Zaniewski, A. M.; Crommie, M. F.; Zettl, A. Graphene as a Long-Term Metal Oxidation Barrier: Worse Than Nothing. *ACS Nano* **2013**, *7*, 5763–5768.
27. Ogletree, D. F.; Carpick, R. W.; Salmeron, M. Calibration of Frictional Forces in Atomic Force Microscopy. *Rev. Sci. Instrum.* **1996**, *67*, 3298.
28. Fabiane, M.; Khamlich, S.; Bello, A.; Dangbegnon, J.; Momodu, D.; Johnson, A. T. C.; Manyala, N. Growth of Graphene Underlayers by Chemical Vapor Deposition. *AIP Adv.* **2013**, *3*, 112126.
29. Ago, H.; Ogawa, Y.; Tsuji, M.; Mizuno, S.; Hibino, H. Catalytic Growth of Graphene: Toward Large-Area Single-Crystalline Graphene. *J. Phys. Chem. Lett.* **2012**, *3*, 2228–2236.
30. Bartelt, N.; McCarty, K. Graphene Growth on Metal Surfaces. *MRS Bull.* **2012**, *37*, 1158–1165.
31. Han, G. H.; Günes, F.; Bae, J. J.; Kim, E. S.; Chae, S. J.; Shin, H.-J.; Choi, J.-Y.; Pribat, D.; Lee, Y. H. Influence of Copper Morphology in Forming Nucleation Seeds for Graphene Growth. *Nano Lett.* **2011**, *11*, 4144–4148.
32. Wofford, J. M.; Nie, S.; McCarty, K. F.; Bartelt, N. C.; Dubon, O. D. Graphene Islands on Cu Foils: The Interplay Between Shape, Orientation, and Defects. *Nano Lett.* **2010**, *10*, 4890–4896.
33. Celebi, K.; Cole, M. T.; Teo, K. B. K.; Park, H. G. Observations of Early Stage Graphene Growth on Copper. *Electrochem. Solid-State Lett.* **2012**, *15*, K1.
34. Hattab, H.; N'Diaye, A. T.; Wall, D.; Klein, C.; Jnawali, G.; Coraux, J.; Busse, C.; van Gastel, R.; Poelsema, B.; Michely, T.; *et al.* Interplay of Wrinkles, Strain, and Lattice Parameter in Graphene on Iridium. *Nano Lett.* **2012**, *12*, 678–682.
35. Obraztsov, A. N.; Obraztsova, E. A.; Tyurnina, A. V.; Zolotukhin, A. A. Chemical Vapor Deposition of Thin Graphite Films of Nanometer Thickness. *Carbon* **2007**, *45*, 2017–2021.
36. Zhang, K.; Arroyo, M. Adhesion and Friction Control Localized Folding in Supported Graphene. *J. Appl. Phys.* **2013**, *113*, 193501.
37. Liu, X.-Z.; Li, Q.; Egberts, P.; Carpick, R. W. Nanoscale Adhesive Properties of Graphene: The Effect of Sliding History. *Adv. Mater. Interface* **2014**, *1*, 1300053.
38. Yoon, T.; Shin, W. C.; Kim, T. Y.; Mun, J. H.; Kim, T.-S.; Cho, B. J. Direct Measurement of Adhesion Energy of Monolayer Graphene As-Grown on Copper and its Application to Renewable Transfer Process. *Nano Lett.* **2012**, *12*, 1448–1452.
39. Filleter, T.; Bennewitz, R. Structural and Frictional Properties of Graphene Films on SiC(0001) Studied by Atomic Force Microscopy. *Phys. Rev. B: Condens. Matter Mater. Phys.* **2010**, *81*, 155412.
40. Egberts, P.; Ye, Z.; Liu, X.-Z.; Dong, Y.; Martini, A.; Carpick, R. W. Environmental Dependence of Atomic-Scale Friction at Graphite Surface Steps. *Phys. Rev. B: Condens. Matter Mater. Phys.* **2013**, *88*, 035409.
41. Gosvami, N. N.; Egberts, P.; Bennewitz, R. Molecular Order and Disorder in the Frictional Response of Alkanethiol Self-Assembled Monolayers. *J. Phys. Chem. A* **2011**, *115*, 6942–6947.
42. Kim, S. M.; Hsu, A.; Lee, Y.-H.; Dresselhaus, M.; Palacios, T.; Kim, K. K.; Kong, J. The Effect of Copper Pre-Cleaning on Graphene Synthesis. *Nanotechnology* **2013**, *24*, 365602.
43. Sader, J. E.; Chon, J. W. M.; Mulvaney, P. Calibration of Rectangular Atomic Force Microscope Cantilevers. *Rev. Sci. Instrum.* **1999**, *70*, 3967.
44. Green, C. P.; Lioe, H.; Cleveland, J.; Proksch, R.; Mulvaney, P.; Sader, J. E. Normal and Torsional Spring Constants of Atomic Force Microscope Cantilevers. *Rev. Sci. Instrum.* **2004**, *75*, 1988.
45. Horcas, I.; Fernández, R.; Gómez-Rodríguez, J. M.; Colchero, J.; Gómez-Herrero, J.; Baro, A. M. WSXM: A Software for Scanning Probe Microscopy and a Tool for Nanotechnology. *Rev. Sci. Instrum.* **2007**, *78*, 013705.